



Research article

Influence of electrolysis conditions on the treatment of herbicide bentazon using artificial UVA radiation and sunlight. Identification of oxidation products



Diego R.V. Guelfi^a, Enric Brillas^b, Fábio Gozzi^a, Amílcar Machulek Jr.^a, Silvio C. de Oliveira^a, Ignasi Sirés^{b,*}

^a Instituto de Química (INQUI), Universidade Federal de Mato Grosso do Sul, 549, Av. Senador Filinto Muller 1555, 79070-900 Campo Grande, Mato Grosso do Sul, Brazil

^b Laboratori d'Electroquímica dels Materials i del Medi Ambient, Departament de Química Física, Facultat de Química, Universitat de Barcelona, Martí i Franquès 1-11, 08028 Barcelona, Spain

ARTICLE INFO

Keywords:

Anodic oxidation
Electro-Fenton
Hydroxyl radical
Pesticide
Solar photoelectro-Fenton

ABSTRACT

The main objective of this work is to demonstrate the viability of solar photoelectro-Fenton (SPEF) process to degrade pesticides in urban wastewater matrix, selecting the herbicide bentazon as a model molecule. In order to provide a correct assessment of the role of the different oxidants and catalysts involved, bentazon was comparatively treated by anodic oxidation with electrogenerated H_2O_2 (AO- H_2O_2), electro-Fenton (EF) and UVA-assisted EF (i.e., PEF) processes as well, either in sulfate or chloride media. Trials were made in a stirred tank reactor with an air-diffusion cathode and a boron-doped diamond (BDD), RuO_2 -based or Pt anode. In chlorinated matrices, the herbicide disappeared more rapidly using a RuO_2 -based anode because of the generated active chlorine. The best mineralization performance was always obtained using BDD due to its higher oxidation power, which allowed the complete destruction of refractory chloroderivatives. A concentration of 0.50 mM Fe^{2+} was found optimal to catalyze Fenton's reaction, largely enhancing the mineralization process under the action of $\cdot\text{OH}$. Among photo-assisted treatments, sunlight was proven superior to a UVA lamp to promote the photolysis of intermediates, owing to its greater UV irradiance and contribution of visible photons, although PEF also allowed achieving a large mineralization. In all cases, bentazon decay obeyed a pseudo-first-order kinetics. SPEF treatment in urban wastewater using BDD at only 16.6 mA cm^{-2} yielded 63.2% mineralization. A thorough, original reaction pathway for bentazon degradation is proposed, including seven non-chlorinated aromatics, sixteen chloroaromatics and two chloroaliphatics identified by GC-MS, most of them not previously reported in literature. Ion-exclusion HPLC allowed the detection of seven short-chain linear carboxylic acids.

1. Introduction

The pollution of hydric resources resulting from anthropogenic activities is of great concern nowadays because it impedes a sustainable development, showing dramatic impact on ecosystems (Boccolini et al., 2013; WWAP, 2017). Agriculture is one of the most prominent human tasks within this framework, owing to the large usage of phytosanitary products that generate toxic and biorecalcitrant wastes in natural water bodies (Islam et al., 2017). Bentazon (3-isopropyl-1H-2,1,3-benzothiadiazin-4(3H)-one-2,2-dioxide, $\text{C}_{10}\text{H}_{12}\text{N}_2\text{O}_3\text{S}$, $M = 240.3 \text{ g mol}^{-1}$) is a selective post-emergence herbicide categorized under the thiadiazine family. It is widely used for controlling the spread of weeds in sorghum, rice, pepper, beans and alfalfa, among others. Several agencies have

documented its potential risk of leaching from soils to natural and even drinking water due to high solubility (about 500 mg L^{-1}), low vapor pressure ($< 10^{-8} \text{ mmHg}$ at 20°C) and large environmental stability (USEPA, 1998; FAO, 1999; WHO, 2017). Up to $120 \mu\text{g L}^{-1}$ have been detected in groundwater of different countries (Köck-Schulmeyer et al., 2014; WHO, 2017), and up to $2.8 \mu\text{g L}^{-1}$ in surface water in Portugal (Rodrigues et al., 2018). Bentazon is not efficiently removed in wastewater treatment plants (Thuy et al., 2008; Loos et al., 2013), which becomes a serious concern because of its toxicity and mutagenic effects on living beings (Galhano et al., 2010; Oliveira et al., 2017). Several advanced oxidation processes (AOPs), which are based on the in-situ production of radical species ($\cdot\text{OH}$, $\text{SO}_4^{\cdot-}$), have been applied to mineralize bentazon, alone or mixed with other herbicides in water,

* Corresponding author.

E-mail address: i.sires@ub.edu (I. Sirés).

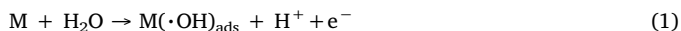
<https://doi.org/10.1016/j.jenvman.2018.10.029>

Received 8 August 2018; Received in revised form 6 October 2018; Accepted 8 October 2018

0301-4797/© 2018 Elsevier Ltd. All rights reserved.

aiming to yield CO_2 , SO_4^{2-} and NO_3^- . $\text{H}_2\text{O}_2/\text{UV}$ (Beltran-Heredia et al., 1996), O_3/UV (Kearney et al., 1987), $\text{O}_3/\text{H}_2\text{O}_2/\text{UV}$ (Lambert et al., 1996), TiO_2/UV (Pelizzetti et al., 1989; Gkika et al., 2004; Pourata et al., 2009; Seck et al., 2013; Schneider et al., 2014; Gholami et al., 2016; Berberidou et al., 2017), $\text{TiO}_2/\text{H}_2\text{O}_2/\text{UV}$ (Mir et al., 2014) and activated persulfate (Wei et al., 2016) have been successfully tested in model solutions prepared with ultrapure water. The removal of bentazon by advanced electrochemical methods (EAOPs) has been limited to the electro-Fenton treatment of synthetic mixtures with chlortoluron and carbofuran in sulfate medium using a carbon-felt cathode (Oturán et al., 2010a,b; Abdessalem et al., 2016). Nonetheless, the performance of photoassisted electrochemical methods applied to bentazon destruction in chlorinated matrices and real wastewater matrices has not been explored so far.

Recently, EAOPs are receiving great attention for wastewater treatment due to their simplicity and high performance to destroy organic pollutants (Comninellis et al., 2008; Brillas et al., 2009; Panizza and Cerisola, 2009; Martínez-Huitle et al., 2015; Moreira et al., 2017). In sulfate medium, the strong oxidant $\cdot\text{OH}$ ($E^0 = 2.8 \text{ V}[\text{SHE}]$) is the main electrogenerated reactive oxygen species (ROS), with ability to cause the gradual mineralization of most organics. The simplest EAOP is anodic oxidation (AO), in which heterogeneous physisorbed $\text{M}(\cdot\text{OH})$ is formed at the anode (M) surface from water discharge, as follows (Panizza and Cerisola, 2009):



Non-active anodes like boron-doped diamond (BDD) tend to be more effective than active ones like Pt and dimensionally stable anodes (DSA[®]) because they produce larger amounts of reactive $\text{M}(\cdot\text{OH})$ (Panizza and Cerisola, 2009; Martínez-Huitle et al., 2015; Moreira et al., 2017). Conversely, in chlorine medium, active chlorine can be electrogenerated from Cl^- oxidation via reaction (2) (De Moura et al., 2014; Moreira et al., 2017). Cl_2 ($E^0 = 1.36 \text{ V}[\text{SHE}]$) predominates up to pH 3, whereas it is transformed to HClO ($E^0 = 1.49 \text{ V}[\text{SCE}]$) via reaction (3) at pH 3–8. The oxidation of Cl^- is favored at active anodes like RuO_2 -based DSA[®] and hence, active chlorine competes with $\cdot\text{OH}$ to oxidize the organics, being detrimental in some cases because toxic and stable chloro-derivatives are accumulated (De Moura et al., 2014; Thiam et al., 2015; Zöllig et al., 2015; Coria et al., 2016; Steter et al., 2016).

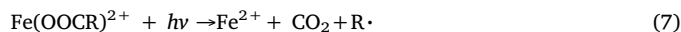
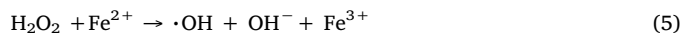


The oxidation ability of AO can be enhanced by promoting the simultaneous electrogeneration of H_2O_2 in an undivided cell, giving rise to the so-called $\text{AO-H}_2\text{O}_2$ process. This oxidant can be directly generated from O_2 reduction at the cathode via reaction (4) using carbonaceous cathodes such as carbon-felt (El-Ghenymy et al., 2014; Abdessalem et al., 2016; Ganzenko et al., 2018; Liu et al., 2018) or hydrophobized carbon black on gas-diffusion substrates (Guelfi et al., 2017, 2018; Lanzalaco et al., 2017; Ridruejo et al., 2018).



From the $\text{AO-H}_2\text{O}_2$ process, significant progress can be made upon addition of a catalytic amount of iron ions to the solution thanks to the occurrence of Fenton's reaction (5). In electro-Fenton (EF) process, organics are destroyed by heterogeneous $\text{M}(\cdot\text{OH})$ and/or active chlorine along with homogeneous $\cdot\text{OH}$ formed from reaction (5), with optimum pH ca. 3 (Brillas et al., 2009; Martínez-Huitle et al., 2015; Olvera-Vargas et al., 2015; dos Santos et al., 2018). The continuous cathodic reduction of Fe^{3+} to Fe^{2+} from reaction (6) propagates Fenton's reaction (5). In photoelectro-Fenton (PEF) with UV light and solar photoelectro-Fenton (SPEF), the UV photons irradiated to the solution can either photolyze complexes of $\text{Fe}(\text{III})$ with organics, like carboxylic acids as shown in reaction (7), or photoreduce the $[\text{Fe}(\text{OH})]^{2+}$ species

to regenerate Fe^{2+} with additional $\cdot\text{OH}$ production via reaction (8) (Zhang et al., 2016; dos Santos et al., 2018; Thiam et al., 2018). The greater irradiance from sunlight compared to artificial UVA light usually leads to a higher performance of SPEF process as compared to PEF (Coria et al., 2018; dos Santos et al., 2018; Murillo-Sierra et al., 2018; Steter et al., 2018). However, the PEF process can be useful in countries exposed to low natural irradiance, or it can be a good alternative at nighttime or during periods with low sunlight intensity. Hence, the oxidation ability of both treatments has to be assessed for a wide variety of organic pollutants in real wastewater.



The aim of this work is to study the influence of the electrolytic conditions in various EAOPs to clarify the role of artificial UVA radiation and sunlight during the PEF and SPEF degradation of bentazon, respectively. $\text{AO-H}_2\text{O}_2$ and EF have been applied under comparable conditions to understand the role of oxidizing agents. Different anode materials have been tested in synthetic sulfate and chloride solutions as well as in urban wastewater. The effect of operation parameters has been assessed to find the optimum mineralization conditions. Aromatic intermediates were identified by gas chromatography-mass spectrometry (GC-MS), whereas final carboxylic acids were detected by high-performance liquid chromatography (HPLC).

2. Materials and methods

2.1. Chemicals

Bentazon ($\geq 99\%$ purity, Pestanal[®]) was purchased from Sigma-Aldrich. Heptahydrate iron(II) sulfate, Na_2SO_4 and NaCl were of analytical grade purchased from Probus. Analytical grade H_2SO_4 and HCl were supplied by Panreac. Carboxylic acids were of analytical grade purchased from Merck and Probus. Most solutions were prepared with ultrapure water (Millipore Milli-Q system, resistivity $> 18.2 \text{ M}\Omega \text{ cm}$ at 25°C).

2.2. Urban wastewater

The urban wastewater sample was obtained from the secondary effluent of a municipal wastewater treatment plant (Gavà-Viladecans, northeastern Spain). Its pH and conductivity were 8.1 and 1.73 mS cm^{-1} , respectively. The total organic carbon (TOC) was 12 mg L^{-1} . The contents of the main ions were: $318 \text{ mg L}^{-1} \text{ Cl}^-$, $141 \text{ mg L}^{-1} \text{ SO}_4^{2-}$, $86 \text{ mg L}^{-1} \text{ Ca}^{2+}$ and $212 \text{ mg L}^{-1} \text{ Na}^+$. The Fe concentration was $< 0.2 \text{ mg L}^{-1}$.

2.3. Electrolytic systems

Solutions of 130 mL were electrolyzed in an undivided tank reactor, open to atmosphere and jacketed to circulate thermostated water at 30°C . All electrolyses were carried out under vigorous stirring with a magnetic follower at 700 rpm. An air-diffusion cathode made of carbon cloth coated with carbon-PTFE supplied by E-TEK was mounted as earlier reported (Guelfi et al., 2017), fed with compressed air at 1 L min^{-1} . This air flowrate leads to the best H_2O_2 generation and allows keeping a dry inner surface, thus preventing the loss of its electroactivity, as occurs in case of flooding. Three different anodes were comparatively tested: (i) RuO_2 -based plate (DSA[®]- Cl_2) purchased from NMT Electrodes, (ii) BDD thin-film over a Si wafer supplied by Neo-Coat, and (iii) Pt sheet (99.99% purity) supplied by SEMPSA. The immersed geometric area of all the electrodes was 3 cm^2 and the

interelectrode spacing was 1 cm. All runs were conducted at constant current density (j) provided by a PAR EG&G 273A potentiostat/galvanostat.

Synthetic solutions with the following salts as electrolytes were tested: (i) 0.050 M Na_2SO_4 , (ii) 0.025 M Na_2SO_4 + 0.035 M NaCl, and (iii) 0.070 M NaCl. The two former media were adjusted to pH 3.0 with H_2SO_4 , whereas HCl was employed for the latter. The conductivity of all solutions was about 7.5 mS cm^{-1} . The runs with urban wastewater were performed after adjusting the pH to 3.0 with H_2SO_4 , ensuring the same conductivity by adding Na_2SO_4 at 0.0047 M.

The AO- H_2O_2 and EF experiments were carried out in the dark. Fe^{2+} concentrations between 0.25 and 1.00 mM (14.0 and 55.8 mg L^{-1}) were employed in EF. The UVA light used for PEF came from a Satellite F6T5BLB blacklight tube, placed 5 cm above the solution. The effective UV irradiance reaching the solution was 5 W m^{-2} , as measured with a Kipp&Zonen CUV 5 UV radiometer. The SPEF trials were performed in clear and sunny days during summer of 2017 in our laboratory at the Universitat de Barcelona (Spain). The solution was directly irradiated with sunlight for four hours from midday with an average UV irradiance close to 31 W m^{-2} , as determined on the same radiometer. In the PEF and SPEF treatments, 0.50 mM Fe^{2+} (27.9 mg L^{-1}) was used as catalyst. Note that in the assays with the urban wastewater, this Fe^{2+} content was actually the catalyst due to the insignificant amount of natural iron ($< 0.2 \text{ mg L}^{-1}$), as stated above. None of the EF, PEF and SPEF trials presented changes in soluble Fe concentration.

2.4. Equipments and analytical procedures

A Crison GLP 22 pH-meter and a Methrom 664 conductometer were employed to measure the pH and conductivity, respectively. All samples, once withdrawn from treated solutions, were filtered with Whatman $0.45 \mu\text{m}$ PTFE filters. The solution TOC was immediately determined on a Shimadzu VCSN TOC analyzer, with L.O.D. = 0.213 mg L^{-1} and L.O.Q. = 0.716 mg L^{-1} . Reproducible TOC values with $\pm 1\%$ accuracy are provided in the Results section. A TNM-1 unit coupled to the TOC system was used to determine the total nitrogen (TN). Bentazon abatement was followed by reversed-phase HPLC. The system included a Waters 600 LC coupled to a Waters 996 detector composed of a photodiode array. The separation was made with a BDS Hypersil C18 $6 \mu\text{m}$, $250 \text{ mm} \times 4.6 \text{ mm}$ column. The methodology involved sample collection (0.5 mL), immediate dilution with acetonitrile (1:1, v/v) to stop the degradation process, and injection into the LC after filtration with a Whatman $0.45 \mu\text{m}$ PTFE filter. A (30:70, v/v) $10 \text{ mM KH}_2\text{PO}_4$ /acetonitrile mixture at pH 3.0 was eluted at 0.8 mL min^{-1} as mobile phase. Bentazon displayed a well-defined peak at retention time of 4.7 min and its concentration was determined at $\lambda = 242 \text{ nm}$, with L.O.D. = 0.094 mg L^{-1} and L.O.Q. = 0.315 mg L^{-1} . The same LC but equipped with an Aminex HPX-87H, $300 \text{ mm} \times 7.8 \text{ mm}$, ion exclusion column was utilized to quantify the generated short-chain linear carboxylic acids at $\lambda = 210 \text{ nm}$. The mobile phase was $4 \text{ mM H}_2\text{SO}_4$ eluted at 0.6 mL min^{-1} . The acids were identified from comparison of their retention times with those of standards.

Trials to assess the mineralization and concentration decays of bentazon were made in duplicate, and average values are given below. Figures also depict the error bars with 95% confidence interval.

The concentrations of NH_4^+ , NO_3^- and SO_4^{2-} ions generated along the treatments, as well as those in urban wastewater, were determined as reported elsewhere (Thiam et al., 2015). The main aromatic products of bentazon were identified by GC-MS from solutions treated by: (i) AO- H_2O_2 with BDD anode in $0.025 \text{ M Na}_2\text{SO}_4$ + 0.035 M NaCl , and (ii) PEF with RuO_2 -based in $0.050 \text{ M Na}_2\text{SO}_4$. The organic components of each sample (about 100 mL) were extracted with CH_2Cl_2 ($3 \times 25 \text{ mL}$) and the resulting organic solution was dried over Na_2SO_4 , filtered and its volume was reduced to about 1 mL for analysis, following the procedure previously described (Steter et al., 2016). Non-polar Teknokroma Sapiens-X5 MS and polar HP INNOWax columns were utilized for GC

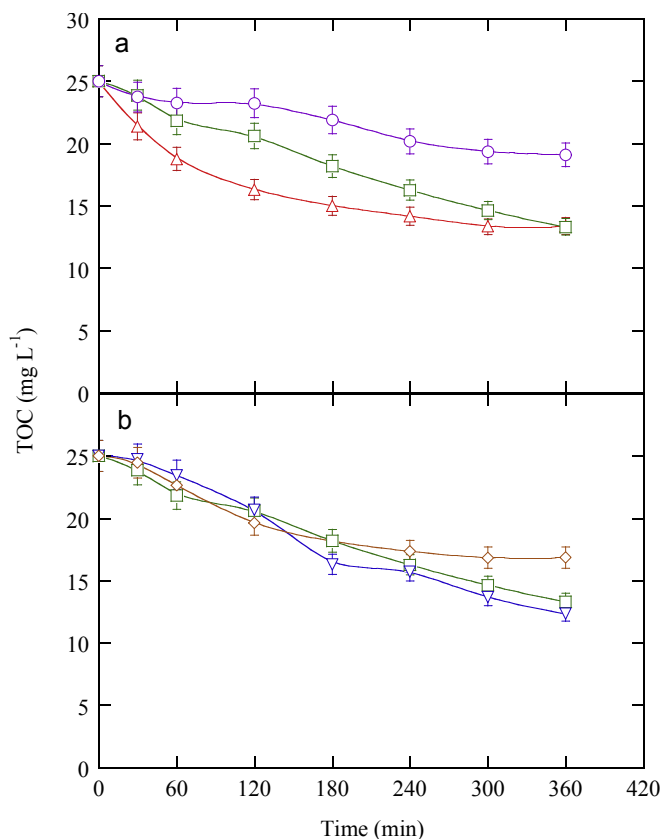


Fig. 1. Change of TOC with electrolysis time for the AO- H_2O_2 treatment of (a) 0.208 mM (50 mg L^{-1}) bentazon solution in $0.025 \text{ M Na}_2\text{SO}_4$ + 0.035 M NaCl at pH 3.0 using as the anode: (Δ) RuO_2 -based, (\circ) Pt and (\square) BDD at $j = 16.6 \text{ mA cm}^{-2}$. In (b), the same herbicide content treated in (∇) $0.050 \text{ M Na}_2\text{SO}_4$, (\square) $0.025 \text{ M Na}_2\text{SO}_4$ + 0.035 M NaCl and (\diamond) 0.070 M NaCl , using a BDD anode.

separation. The mass spectra were identified by means of NIST05-MS database.

3. Results and discussion

3.1. AO- H_2O_2 treatment of bentazon solutions in ultrapure water

First, the ability of different anodes to electrogenerate $\text{M}(\cdot\text{OH})$ and active chlorine by AO- H_2O_2 in $0.025 \text{ M Na}_2\text{SO}_4$ + 0.035 M NaCl was assessed from TOC decays, in order to obtain information about the attack of these oxidants on the mixture of bentazon and its oxidation by-products. Fig. 1a illustrates the TOC-time plots found during these trials at pH 3.0 upon application of 16.6 mA cm^{-2} for 360 min. A slow TOC decay can be observed in all cases, which was enhanced in the order: Pt < BDD < RuO_2 -based anode, attaining an abatement of 23.6%, 46.8% and 46.9% at the end of the electrolysis, respectively. The higher oxidation ability of the metal oxide anode can be ascribed to its larger ability to produce active chlorine, mainly as HClO (Zöllig et al., 2015; Coria et al., 2016; Steter et al., 2016), which can gradually mineralize the organics. The BDD anode generates lower amounts of active chlorine, although the BDD($\cdot\text{OH}$) is much more powerful than the $\text{RuO}_2(\cdot\text{OH})$ (Panizza and Cerisola, 2009; Thiam et al., 2015; Steter et al., 2016). As a result, the radical adsorbed on BDD can also gradually remove the organic compounds. It is noticeable that, at 360 min of both treatments, the same mineralization degree (about 47%) was obtained, suggesting that chloroderivatives formed upon chlorination are continuously destroyed by BDD($\cdot\text{OH}$), whereas they are more resistant to active chlorine produced as main oxidant with the RuO_2 -

based anode. In the case of Pt, Fig. 1a depicts a much slower TOC decay. This is not surprising, considering its smaller ability to oxidize Cl^- as compared to the used DSA[®] and the poor oxidation power of $\text{Pt}(\cdot\text{OH})$ (Panizza and Cerisola, 2009; Coria et al., 2016).

To better understand the role of the generated oxidizing agents, another series of trials was carried out with the BDD anode, using three different media prepared with ultrapure water. Fig. 1b shows a slight enhancement of TOC removal in 0.050 M Na_2SO_4 as compared to 0.025 M Na_2SO_4 + 0.035 M NaCl, achieving 50.6% vs. 46.8% mineralization at 360 min. In 0.070 M NaCl, however, TOC was only reduced by 31% at 180 min, reaching a quasi-steady value. This can be explained by the formation of a large quantity of chloroderivatives in the presence of active chlorine electrogenerated to a large extent. Since $\text{BDD}(\cdot\text{OH})$ destruction is promoted by reaction with Cl^- , yielding much less reactive radicals (Panizza and Cerisola, 2009; Martínez-Huitle et al., 2015), such chloro-organics remained quite stable in solution. Much smaller amounts of such persistent products were formed in 0.025 M Na_2SO_4 + 0.035 M NaCl. This, combined with the lower destruction of $\text{BDD}(\cdot\text{OH})$ by Cl^- , allowed a more effective degradation of the organic matter, showing a mineralization profile similar to that found in 0.050 M Na_2SO_4 where this radical is the main oxidant. These findings indicate that increasing the Cl^- content is detrimental for bentazon mineralization by $\text{AO-H}_2\text{O}_2$ due to the accumulation of persistent chlorinated by-products. In this kind of process, BDD exhibited the greatest performance, as confirmed from the fact that almost 0% and < 10% of TOC were removed from solutions with 0.208 mM herbicide in 0.050 M Na_2SO_4 after 360 min using RuO_2 -based or Pt anode, respectively (not shown).

3.2. EF treatment of bentazon solutions in ultrapure water

The EF treatment of 0.208 mM bentazon solutions was studied in 0.050 M Na_2SO_4 at pH 3.0 to assess the oxidation ability of homogeneous $\cdot\text{OH}$ formed from Fenton's reaction (5) in the absence of active chlorine. First, the effect of key operation parameters like Fe^{2+} concentration and j was assessed using the RuO_2 -based anode, which can be considered as an inert material in terms of mineralization capacity in this medium, as stated above. Fig. 2a shows the change of TOC of the solution with 0.25–1.00 mM Fe^{2+} at 16.6 mA cm^{-2} . The highest mineralization rate was obtained with 0.50 mM Fe^{2+} , eventually attaining a TOC reduction of 31.6%. The enhanced mineralization upon increase from 0.25 to 0.50 mM Fe^{2+} can be accounted for by the concomitant acceleration of Fenton's reaction (5). In contrast, the excessive consumption of $\cdot\text{OH}$ by reaction with Fe^{2+} at 1.00 mM via reaction (9) justifies the observed deceleration (Brillas et al., 2009; Panizza and Cerisola, 2009; Martínez-Huitle et al., 2015). Based on this, 0.50 mM Fe^{2+} was taken as the optimal concentration for subsequent experiments.



Fig. 2b presents the time course of TOC for the above solution with 0.50 mM Fe^{2+} at j values ranging between 3.3 and 100 mA cm^{-2} . As expected, the rise of j allowed a larger H_2O_2 electrogeneration at the cathode, thereby accelerating the mineralization owing to the promotion of Fenton's reaction (5) (Martínez-Huitle et al., 2015; Olvera-Vargas et al., 2015; Guelfi et al., 2018). It is remarkable that at 3.3 mA cm^{-2} , TOC was kept practically constant because of the very small H_2O_2 generation. In contrast, at 16.6 mA cm^{-2} , the H_2O_2 content was high enough to reduce the TOC by 31.6%, becoming 41.6% at 100 mA cm^{-2} . Nevertheless, Fig. 2b evidences a drastic deceleration of TOC removal as the applied j was increased, suggesting the formation of hardly oxidizable products by homogeneous $\cdot\text{OH}$.

Then, the influence of the heterogeneous $\text{M}(\cdot\text{OH})$ electrogenerated at different anode surfaces on the mineralization rate in EF process was evaluated at 100 mA cm^{-2} . As can be observed in Fig. 2c, TOC was

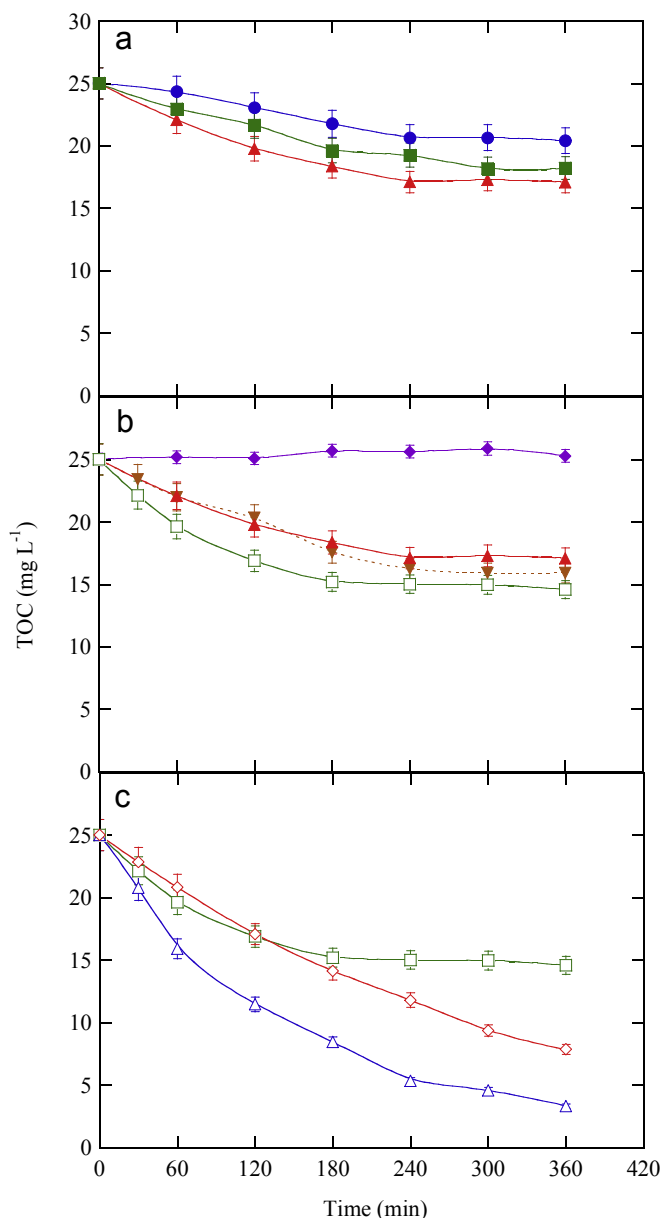


Fig. 2. TOC decay vs. electrolysis time for the EF treatment of 0.208 mM bentazon solution in 0.050 M Na_2SO_4 at pH 3.0 using the (a) RuO_2 -based DSA[®] at $j = 16.6 \text{ mA cm}^{-2}$ and $[\text{Fe}^{2+}]$: (●) 0.25 mM, (▲) 0.50 mM and (■) 1.00 mM. In (b), the same anode and 0.50 mM Fe^{2+} , at j : (◆) 3.33 mA cm^{-2} , (▲) 16.6 mA cm^{-2} , (▼) 33.3 mA cm^{-2} and (□) 100 mA cm^{-2} . In (c), the same solution with 0.50 mM Fe^{2+} at $j = 100 \text{ mA cm}^{-2}$, using as the anode: (□) RuO_2 -based, (◇) Pt and (△) BDD.

more rapidly abated in the anode order: RuO_2 -based < Pt < BDD, attaining a final decay of 41.6%, 68.4% and 86.8%, respectively. In contrast to that explained above in the case of the RuO_2 -based anode, a gradual TOC decay can be seen in Fig. 2c for the other two anodes, meaning that intermediates can be continuously removed by the combined action of $\cdot\text{OH}$ and $\text{M}(\cdot\text{OH})$. The superiority of BDD anode can then be related to the much greater oxidation power of $\text{BDD}(\cdot\text{OH})$ as compared to $\text{Pt}(\cdot\text{OH})$ (Martínez-Huitle et al., 2015; Coria et al., 2016; Steter et al., 2016).

3.3. Photo-assisted treatments of bentazon solutions

The first study about the PEF process was focused on the treatment of the 0.208 mM herbicide solutions in 0.050 M Na_2SO_4 with 0.50 mM

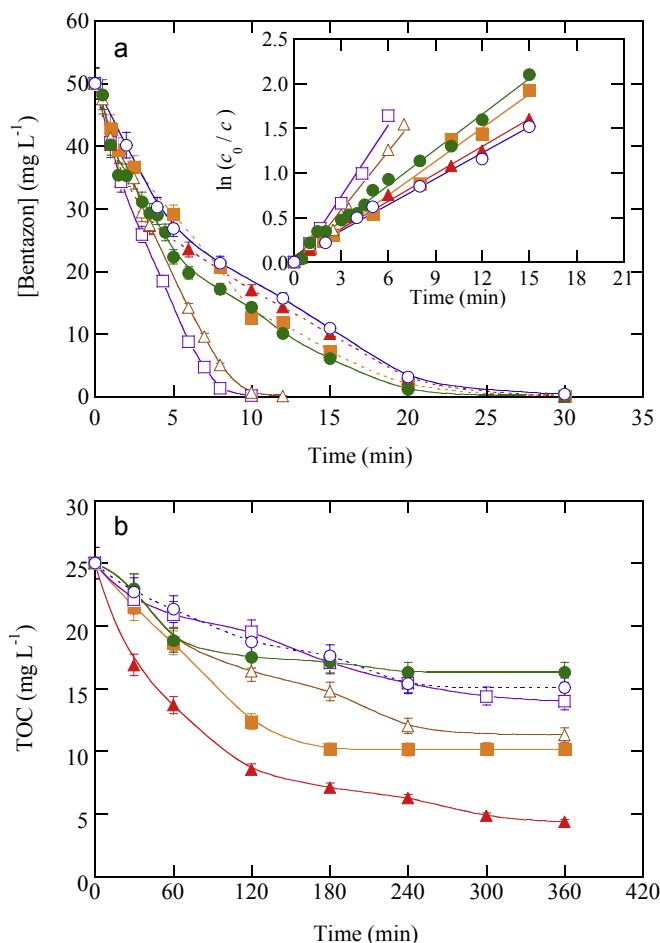


Fig. 3. Change of (a) bentazon concentration and (b) TOC with electrolysis time for the PEF treatment of 130 mL of 0.208 mM herbicide solution with 0.50 mM Fe²⁺ at pH 3.0 using an air-diffusion cathode at $j = 16.6 \text{ mA cm}^{-2}$ under irradiation with a 6 W UVA lamp. Anode: (■, □) RuO₂-based, (▲, △) BDD and (●, ○) Pt. Electrolyte: (■, ▲, ●) 0.050 M Na₂SO₄ and (□, △, ○) 0.025 M Na₂SO₄ + 0.035 M NaCl. The pseudo-first-order kinetic analysis for bentazon abatement is presented in the inset panel of (a).

Fe²⁺ at pH 3.0 and 16.6 mA cm^{-2} . Fig. 3a illustrates the quite similar bentazon abatements obtained regardless of the anode under these conditions, completely disappearing in about 30 min. This behavior can be ascribed to the pre-eminent oxidation of the herbicide with homogeneous $\cdot\text{OH}$ formed from Fenton's reaction (5) in all cases, with little influence of the heterogeneous M($\cdot\text{OH}$). Kinetic analysis of the concentration decays showed a good agreement with a pseudo-first-order reaction (see the inset of Fig. 3a), allowing the determination of apparent rate constant (k_1) values of $0.10\text{--}0.13 \text{ min}^{-1}$ with R -squared values close to 0.990. This kinetic behavior suggests the generation of a steady and small concentration of $\cdot\text{OH}$, which reacts with bentazon. It is worth noting that similar k_1 -values were also found under comparable EF treatments (data not shown), suggesting the irrelevance of photolytic reaction (8) to produce additional amounts of $\cdot\text{OH}$.

Fig. 3a also shows the degradation of the herbicide in 0.025 M Na₂SO₄ + 0.035 M NaCl under analogous conditions. The combined oxidation by both, active chlorine and $\cdot\text{OH}$, allowed a faster bentazon removal in PEF with BDD, being its decay even more rapid with the RuO₂-based anode owing to the greater formation of active chlorine, leading to total removal after 12 and 10 min, respectively. In contrast, the use of a Pt anode did not enhance the herbicide abatement, thus confirming its low ability to produce active chlorine. The inset of Fig. 3a evidences a pseudo-first-order kinetic decay in all these treatments, showing increasing k_1 -values of 0.10 min^{-1} ($R^2 = 0.989$) with

Pt, 0.22 min^{-1} ($R^2 = 0.985$) with BDD and 0.26 min^{-1} ($R^2 = 0.987$) with the DSA[®]. Based on this, it can be stated that the herbicide underwent the attack of a constant and low content of generated active chlorine and/or $\cdot\text{OH}$.

A very different behavior can be observed in Fig. 3b for the corresponding TOC abatements. The mineralization achieved in 0.050 M Na₂SO₄ was quicker than that found in 0.025 M Na₂SO₄ + 0.035 M NaCl. Furthermore, in both media, TOC was more rapidly abated in the anode sequence: Pt < RuO₂-based < BDD. The superiority of BDD over the other anodes corroborated the results described for AO-H₂O₂ and EF. At 16.6 mA cm^{-2} using 0.050 M Na₂SO₄, for example, it yielded 50.6% of TOC removal in AO-H₂O₂ (see Fig. 1b), which was enhanced up to 82.4% in PEF (see Fig. 3b). This greater mineralization ability can be related to: (i) the additional oxidation with homogeneous $\cdot\text{OH}$, and (ii) photodecomposition of intermediates, like Fe(III)-carboxylate complexes from reaction (7), under UVA irradiation. In 0.025 M Na₂SO₄ + 0.035 M NaCl, the formation of persistent chloroderivatives was strongly detrimental. Therefore, only 54.8% of TOC was removed after 360 min in PEF (see Fig. 3b), being slightly higher than 46.8% determined in AO-H₂O₂ (see Fig. 1b), which informs about the large resistance of such by-products to $\cdot\text{OH}$ and UVA light. BDD was chosen as the most suitable anode for SPEF assays.

The treatment of 0.208 mM bentazon solutions in 0.050 M Na₂SO₄ at pH 3.0 by SPEF with BDD was carried out at different j values for 240 min. Fig. 4a reveals that the herbicide was completely abated after 120 min at a very low $j = 3.33 \text{ mA cm}^{-2}$, whereas it disappeared in 20 and 8 min operating at 16.6 and 100 mA cm^{-2} , respectively. It is worth highlighting that at 16.6 mA cm^{-2} , the herbicide degradation by SPEF was faster than by PEF (see Fig. 3a), requiring only 20 min instead of 30 min for total removal. This was corroborated by the greater k_1 -values found for SPEF, yielding 0.026 min^{-1} ($R^2 = 0.992$) at 3.33 mA cm^{-2} , 0.16 min^{-1} ($R^2 = 0.993$) at 16.6 mA cm^{-2} and 0.47 min^{-1} ($R^2 = 0.985$) at 100 mA cm^{-2} , as obtained from the excellent linear correlations shown in the inset of Fig. 4a. This phenomenon can be accounted for by the participation of $\cdot\text{OH}$ induced by photolytic reaction (8), which is particularly promoted due to the much larger irradiance from sunlight as compared to the UVA lamp. This also accelerated the formation and further photolysis of photoactive intermediates, strongly enhancing the mineralization process, as shown in Fig. 4b for the above trials. TOC was reduced by 82.4%, 89.2% and 96.0% after 240 min at 3.33 , 16.6 and 100 mA cm^{-2} , respectively. The almost total mineralization reached at 100 mA cm^{-2} is an indication of the powerful synergistic action of BDD($\cdot\text{OH}$), $\cdot\text{OH}$ and sunlight to destroy the herbicide and its reaction by-products.

SPEF with BDD anode was further employed to treat 0.208 mM bentazon spiked into 0.025 M Na₂SO₄ + 0.035 M NaCl or urban wastewater. The latter matrix contained up to 12 mg L^{-1} of natural organic matter (NOM), primordially composed of fulvic and humic acids. Fig. 5a shows the degradation of the herbicide in the presence of 0.50 mM Fe^{2+} , adjusting the pH to 3.0 and working at 16.6 mA cm^{-2} . In synthetic chloride medium, the herbicide was very rapidly abated in 15 min, somewhat shorter than 20 min required in 0.050 M Na₂SO₄ (see Fig. 4a). This confirms the more effective attack of $\cdot\text{OH}$ in the absence of Cl⁻ since it minimizes its conversion to less oxidizing chlorinated radicals (Thiam et al., 2015; Steter et al., 2016). Fig. 5a highlights similar bentazon decay in urban wastewater during the first 10 min, whereupon it was decelerated to finally disappear at 45 min. This phenomenon can be ascribed to the simultaneous consumption of part of the generated oxidizing agents to destroy the NOM. The pseudo-first-order kinetic analysis shown in the inset of Fig. 5a corroborates the analogous concentration removal at the beginning of the treatments, yielding $k_1 = 0.11 \text{ min}^{-1}$ ($R^2 = 0.992$) in 0.025 M Na₂SO₄ + 0.035 M NaCl and $k_1 = 0.096 \text{ min}^{-1}$ ($R^2 = 0.986$) in urban wastewater. The corresponding normalized TOC abatement is depicted in Fig. 5b. A greater mineralization degree with 80.2% TOC reduction at 240 min was achieved in 0.025 M Na₂SO₄ + 0.035 M NaCl, as compared to

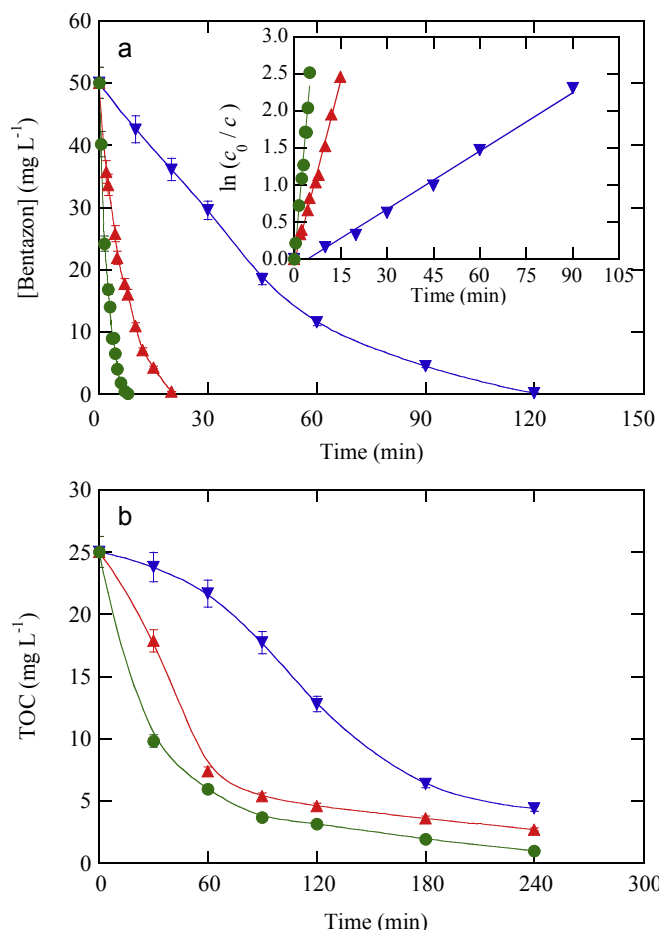


Fig. 4. (a) Herbicide concentration and (b) TOC abatements vs. electrolysis time for the SPEF treatment of 130 mL of a 0.208 mM bentazon solution in 0.050 M Na₂SO₄ with 0.50 mM Fe²⁺ at pH 3.0 using a BDD/air-diffusion cell at j : (▼) 3.3 mA cm⁻², (▲) 16.6 mA cm⁻² and (●) 100 mA cm⁻². In (a), kinetic analysis assuming a pseudo-first-order reaction for the herbicide.

63.2% found in urban wastewater. However, note that 20.1 mg L⁻¹ of TOC were removed in the former matrix, whereas a greater amount of 23.4 mg L⁻¹ was destroyed in the latter one. This means that the SPEF process is able to mineralize both, the herbicide and the NOM in urban wastewater.

3.4. Mineralization current efficiency

At the end of the PEF treatment of the 0.208 mM bentazon solution in 0.050 M Na₂SO₄ at 16.6 mA cm⁻², which yielded 89.2% mineralization, the released inorganic ions were identified and quantified. It was found that near 99% of the initial S (6.66 mg L⁻¹) was converted into SO₄²⁻ ion, whereas the initial N (5.82 mg L⁻¹) was transformed into 0.96 mg L⁻¹ NH₄⁺ (12.8%) and 18.68 mg L⁻¹ NO₃⁻ (71.7%). This agrees with the reported conversion of the heteroatoms of bentazon mainly into SO₄²⁻ and NO₃⁻ from different AOPs (Pelizzetti et al., 1989; Beltran-Heredia et al., 1996; Oturan et al., 2010a; Seck et al., 2013; Mir et al., 2014; Steter et al., 2016; Berberidou et al., 2017). Moreover, the soluble TN decayed to 5.02 mg L⁻¹, indicating that 13.7% of the initial N was released as volatile species, probably N₂ and N_xO_y as proposed for other nitrogenated compounds (Guelfi et al., 2017; dos Santos et al., 2018).

From these findings, the theoretical total mineralization reaction of bentazon, with a number of carbon atoms (m) of 10, yielding CO₂ and SO₄²⁻ and NO₃⁻ as main ions, with a number of consumed electrons (n) of 62, can be written as follows:

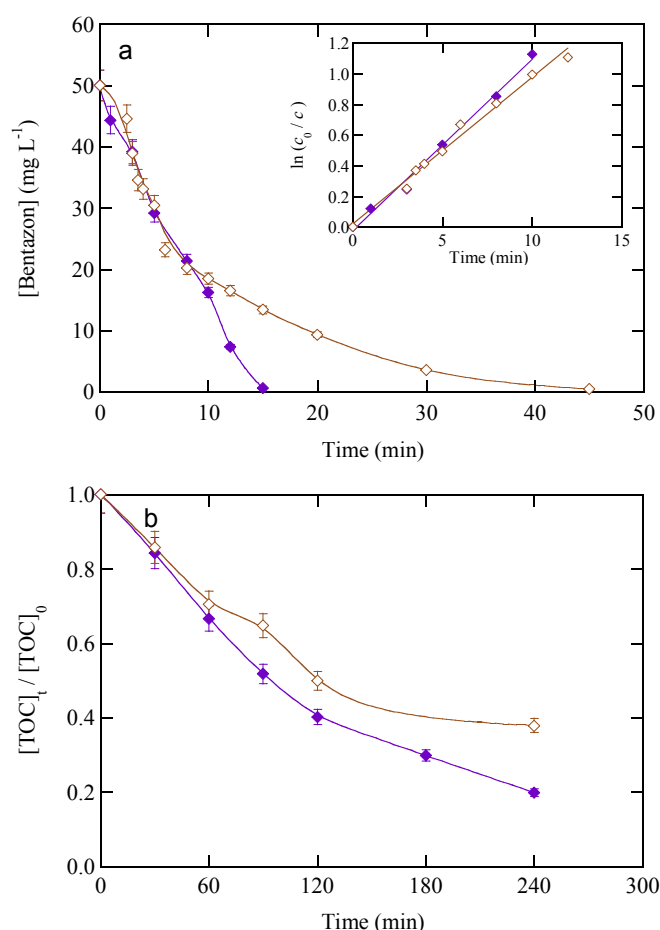
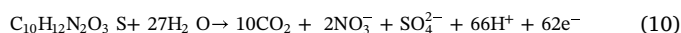


Fig. 5. (a) Herbicide concentration decay and pseudo-first-order kinetic analysis, and (b) normalized TOC removal with electrolysis time for the SPEF treatment of 130 mL of 0.208 mM bentazon spiked into (◆) ultrapure water with 0.025 M Na₂SO₄ + 0.035 M NaCl ([TOC]₀ = 25 mg L⁻¹) and (◇) urban wastewater with 0.0047 M Na₂SO₄ ([TOC]₀ = 37 mg L⁻¹), both with 0.50 mM Fe²⁺, at pH 3.0. The treatments were performed with a BDD/air-diffusion cell at j = 16.6 mA cm⁻².



Taking into account the experimental TOC abatement (ΔTOC , in mg L⁻¹) for a synthetic solution in ultrapure water at current I (in A), the mineralization current efficiency (MCE, in %) at a given electrolysis time (in h) was estimated from Eq. (11) (Brillas et al., 2009; Martínez-Huitle et al., 2015; Moreira et al., 2017):

$$\% MCE = \frac{n F V \Delta TOC}{4.32 \times 10^7 m I t} \times 100 \quad (11)$$

where 4.32×10^7 is a conversion factor to homogenize the units ($3600 \text{ s h}^{-1} \times 12,000 \text{ mg C mol}^{-1}$), V is the solution volume (in L) and F is the Faraday constant.

Fig. 6a–c presents the MCE values determined for the assays of Figs. 2c, 3b, 4b and 5b. According to Eq. (11), two tendencies can be observed: (i) greater MCE as more TOC was removed at the same j value, and (ii) decrease of MCE at increasing j (i.e., I), despite the enhancement of ΔTOC . This latter phenomenon can be related to the concomitant acceleration of parasitic reactions of oxidizing agents, e.g., conversion of $M(\cdot OH)$ into O₂ or scavenging of $\cdot OH$ by H₂O₂, with the consequent relative decay of reactions with organics (Brillas et al., 2009; Martínez-Huitle et al., 2015; Moreira et al., 2017). The former tendency can be deduced from Fig. 6a and b, when the three anodes (RuO₂-based, BDD and Pt) were comparatively used for EF in 0.050 M Na₂SO₄ at 100 mA cm⁻² and PEF using the same medium and 0.025 M

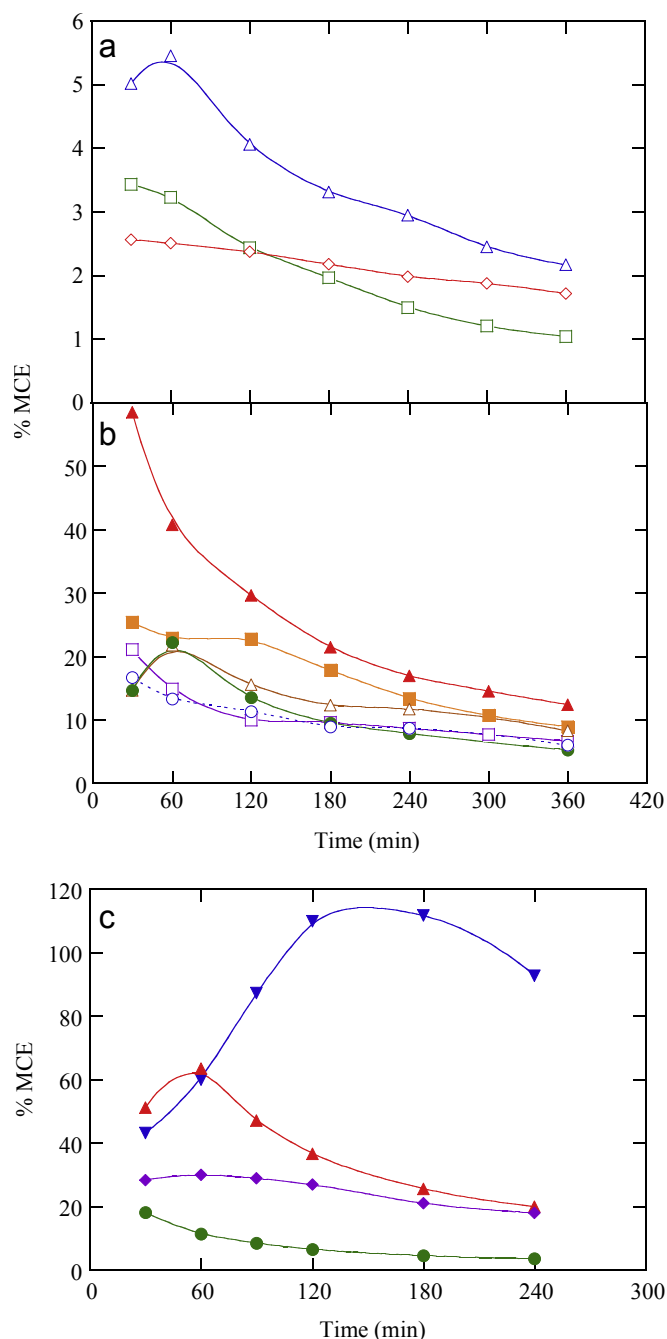


Fig. 6. Mineralization current efficiency determined for the assays of (a) Fig. 2c, (b) Fig. 3b and (c) Figs. 4b and 5b (ultrapure water).

$\text{Na}_2\text{SO}_4 + 0.035\text{M NaCl}$ at 16.6 mA cm^{-2} , respectively. In both figures, BDD is confirmed as the best anode always attaining the highest MCE values regardless of the EAOP and matrix considered. Furthermore, most of the MCE-time plots presented a maximal at short electrolysis time, followed by a continuous decay of MCE because of the abatement of the organic load with formation of more persistent products (Panizza and Cerisola, 2009; Martínez-Huitle et al., 2015). The decrease of MCE with raising j can be seen in Fig. 6c during the SPEF treatments with BDD in $0.050 \text{ M Na}_2\text{SO}_4$. A maximal of 111% MCE at 120–180 min working at 3.3 mA cm^{-2} was found, dropping to 93% at 240 min. Conversely, at 100 mA cm^{-2} , which yielded a much greater TOC removal of 96.0%, smaller MCE values progressively decaying from 18% to 3.6% were obtained. The high MCE values, even $> 100\%$,

determined at the lowest j can be explained by the contribution of photolytic reactions under sunlight irradiation, which is a parameter not considered for calculation in Eq. (11). In addition, Fig. 6c shows lower MCE values for SPEF in $0.025 \text{ M Na}_2\text{SO}_4 + 0.035 \text{ M NaCl}$ at 16.6 mA cm^{-2} due to the persistence of chloroderivatives. This effect on MCE is also seen in Fig. 6b for all anodes when the data in different media are compared.

3.5. Detection of aromatic by-products and final carboxylic acids

Fig. 7 presents seven non-chlorinated aromatics formed upon oxidation with $\cdot\text{OH}$, along with sixteen chlorinated aromatics and two chlorinated aliphatics generated by the simultaneous attack of active chlorine. To simplify, the m/z values given for the chlorinated compounds correspond to those considering the ^{35}Cl isotope. All these products were identified during the degradation of solutions containing 0.208 mM herbicide either in $0.050 \text{ M Na}_2\text{SO}_4$ by PEF with RuO_2 -based anode or in $0.025 \text{ M Na}_2\text{SO}_4 + 0.035 \text{ M NaCl}$ by $\text{AO-H}_2\text{O}_2$ with BDD. In the non-chlorinated matrix, a derivative with m/z 254 from addition of hydroxyl to the benzenic ring of bentazon (m/z 240) with formation of a $\text{C}=\text{C}$ -bond in the lateral isopropyl group was detected. The cleavage of the benzothiadiazine structure with loss of SO_4^{2-} ion and consecutive oxidation of the N atom bonded to the benzenic ring with increasing demethylation of the isopropyl group yielded the compounds with m/z 208, 180 and 149, which were subsequently attacked by $\cdot\text{OH}$ leading to products with m/z 179, 194 and 138, respectively. On the other hand, in the chlorinated matrix, chlorination along with hydroxylation of bentazon yielded compounds with m/z 288, 274 and 308. Again, the cleavage of the benzothiadiazine group with loss of SO_4^{2-} ion followed by $\cdot\text{OH}$ /active chlorine attack originated four chlorinated products with m/z 213, 247, 248 and 315 containing the isopropyl group, along with other three compounds with m/z 198, 184 and 170 in which this group was progressively demethylated. Further oxidation of the former derivative yielded two products, with m/z 214 and 196, whereas the second one evolved to compounds with m/z 200 and 253 and the third one to a product with m/z 200. In addition, the simplest chlorinated aromatic with m/z 179 and two aliphatics with m/z 188 and 107 were also formed. It is noticeable that the chlorinated products shown in Fig. 7 have not been previously reported in the literature since bentazon degradation was not studied in a chlorinated matrix, whereas only the aromatic product with m/z 208 detected in sulfate medium has been described for the herbicide treatment pon $\text{TiO}_2/\text{H}_2\text{O}_2/\text{UV}$ (Mir et al., 2014).

The above aromatic derivatives are expected to yield short-chain linear carboxylic acids from the cleavage of the benzene moiety (Olvera-Vargas et al., 2015; Coria et al., 2018; dos Santos et al., 2018; Thiam et al., 2018). This was confirmed from the ion-exclusion HPLC analysis of a 0.208 mM bentazon solution in $0.050 \text{ M Na}_2\text{SO}_4$ with 0.50 mM Fe^{2+} at pH 3.0 treated by SPEF with BDD at 16.6 mA cm^{-2} . Seven acids including tartaric, maleic, fumaric, malonic, formic, oxalic and oxamic were detected. The six former acids can be originated from the breakage of the benzenic ring of aromatic intermediates, whereas oxamic acid comes from the oxidation of N-derivatives. This latter acid, along with oxalic and formic are directly mineralized to CO_2 (Brillas et al., 2009; Martínez-Huitle et al., 2015; Moreira et al., 2017). It should be noted that under the SPEF conditions tested, all these acids formed Fe(III) complexes that were susceptible to be photodecomposed via reaction (7).

Fig. 8 illustrates the time course of all the detected acids, which persisted in the medium until 180 min as maximal. These products were accumulated up to maximum contents between 0.51 and 5.24 mg L^{-1} in ca. 30 min, to be subsequently destroyed under the oxidative action of $\text{BDD}(\cdot\text{OH})$ and $\cdot\text{OH}$ and, more largely, upon photolysis of their Fe(III) complexes. These findings indicate that after 240 min of this SPEF treatment (see Fig. 4b), the 10.8% of the initial remaining TOC must be ascribed to the accumulation of persistent unidentified by-products,

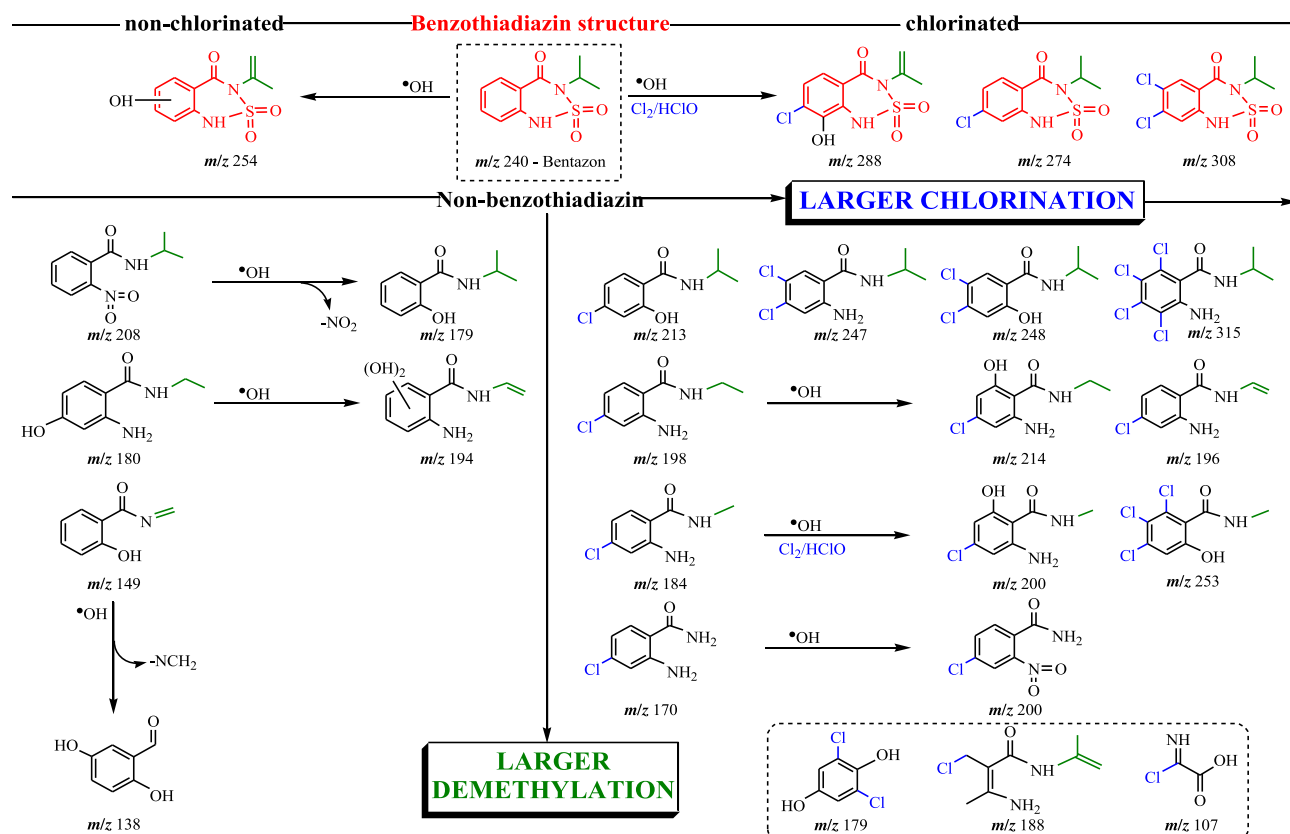


Fig. 7. Molecular structures of intermediates, formed upon demethylation, hydroxylation and chlorination processes, proposed for the degradation of bentazon during the electrochemical treatments under the action of $\cdot\text{OH}$ and/or active chlorine.

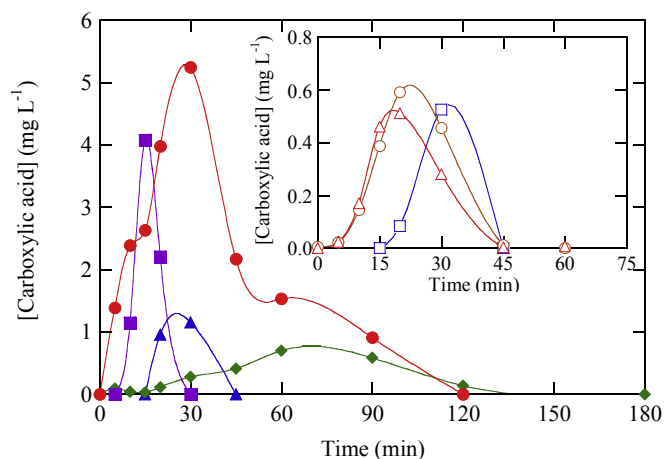


Fig. 8. Concentration of carboxylic acids vs. electrolysis time detected during the SPEF treatment of 130 mL of a solution with 0.208 mM bentazon, 0.050 M Na_2SO_4 and 0.50 mM Fe^{2+} at pH 3.0 using a BDD/air-diffusion cell at $j = 16.6 \text{ mA cm}^{-2}$. Acids: (▲) tartaric, (◆) oxamic, (■) malonic and (●) formic. Inset: (□) oxalic, (○) maleic and (△) fumaric.

which are even more hardly oxidizable than the final carboxylic acids, thus impeding the total mineralization of the herbicide solution.

4. Conclusions

The non-active BDD anode showed its superiority over active RuO_2 -based and Pt anodes and, combined with an air-diffusion cathode, gave rise to the greatest mineralization of bentazon in synthetic sulfate and chloride media by $\text{AO-H}_2\text{O}_2$, EF, PEF and SPEF. This is due to the greater oxidation power of $\text{BDD}(\cdot\text{OH})$ as compared to $\text{RuO}_2(\cdot\text{OH})$ and

$\text{Pt}(\cdot\text{OH})$, particularly demonstrated from its ability to destroy persistent chloroderivatives. The homogeneous $\cdot\text{OH}$ generated from Fenton's reaction enhanced the herbicide mineralization, yielding a similar herbicide decay in EF and PEF at an optimum Fe^{2+} concentration of 0.50 mM at pH 3.0. In chlorinated matrices, bentazon disappeared more rapidly using a RuO_2 -based anode thanks to the generated active chlorine, although BDD was more effective to destroy the chloroderivatives. A pseudo-first-order kinetics for bentazon was found in all these EAOPs. The PEF process with BDD in sulfate medium allowed a high TOC decay of 86.8% at 100 mA cm^{-2} , although SPEF with BDD became the most powerful treatment with 96.0% TOC reduction. The same treatment in urban wastewater at 16.6 mA cm^{-2} yielded 63.2% mineralization, showing the removal of the herbicide along with NOM. This work allows concluding that SPEF and PEF could be viable for the treatment of urban wastewater polluted with bentazon. Seven non-chlorinated aromatics, sixteen chloro-aromatics and two chloro-aliphatics were detected as main intermediates, along with seven non-chlorinated aliphatic acids, most of them not reported in earlier works.

Acknowledgements

Financial support from project CTQ2016-78616-R (AEI/FEDER, EU) as well as from FUNDECT, CAPES and CNPq (Brazil), is acknowledged.

References

- Abdesslem, A., Oturan, N., Bellakhal, N., Oturan, M.A., Dachraoui, M., 2016. Remediation of water contaminated with pesticides by indirect electrochemical oxidation process electro-Fenton. *J. Adv. Oxid. Technol.* 11, 276–282.
- Beltran-Heredia, J., Benitez, F.J., Gonzalez, T., Acero, J.L., Rodriguez, B., 1996. Photolytic decomposition of bentazon. *J. Chem. Technol. Biotechnol.* 66, 206–212.
- Berberidou, C., Kitsiou, V., Kazala, E., Lambropoulou, D.A., Kouras, A., Kosma, C.I., Albanis, T.A., Poullos, I., 2017. Study of the decomposition and detoxification of the

- herbicide bentazon by heterogeneous photocatalysis: kinetics, intermediates and transformation pathways. *Appl. Catal. B: Environ.* 200, 150–163.
- Boccolini, M.P., Boccolini, C.S., Chrisman, R.J., Markowitz, S.B., Koifman, S., Koifman, R.J., Meyer, A., 2013. Pesticide use and non-Hodgkin's lymphoma mortality in Brazil. *Int. J. Hyg. Environ. Health* 216, 461–466.
- Brillas, E., Sirés, I., Oturan, M.A., 2009. Electro-Fenton process and related electrochemical technologies based on Fenton's reaction chemistry. *Chem. Rev.* 109, 6570–6631.
- Comminellis, C., Kapalka, A., Malato, S., Parsons, S.A., Poullos, I., Mantzavinos, D., 2008. Advanced oxidation processes for water treatment: advances and trends for R&D. *J. Chem. Technol. Biotechnol.* 83, 769–776.
- Coria, G., Sirés, I., Brillas, E., Nava, J.L., 2016. Influence of the anode material on the degradation of naproxen by Fenton-based electrochemical processes. *Chem. Eng. J.* 304, 817–825.
- Coria, G., Pérez, T., Sirés, I., Brillas, E., Nava, J.L., 2018. Abatement of the antibiotic levofloxacin in a solar photoelectro-Fenton flow plant: modeling the dissolved organic carbon concentration-time relationship. *Chemosphere* 198, 174–181.
- De Moura, D.C., De Araújo, C.K.C., Zanta, C.L., Salazar, R., Martínez-Huitle, C.A., 2014. Active chlorine species electrogenerated on Ti/Ru_{0.3}Ti_{0.7}O₂ surface: electrochemical behavior, concentration determination and their application. *J. Electroanal. Chem.* 731, 145–152.
- dos Santos, A.J., Martínez-Huitle, C.A., Sirés, I., Brillas, E., 2018. Use of Pt and BDD anodes in the electrochemical advanced oxidation of Ponceau SS diazo dye in acidic sulfate medium. *ChemElectroChem* 5, 685–693.
- El-Ghenymy, A., Rodríguez, R.M., Brillas, E., Oturan, N., Oturan, M.A., 2014. Electro-Fenton degradation of the antibiotic sulfanilamide with Pt/carbon-felt and BDD/carbon-felt cells. Kinetics, reaction intermediates, and toxicity assessment. *Environ. Sci. Pollut. Res.* 21, 8368–8378.
- FAO, 1999. Specifications and Evaluations for Plant Protection Products. Available in: http://www.fao.org/fileadmin/templates/agphome/documents/Pests_Pesticides/Specs/bentazon.pdf (last accessed 2017).
- Galhano, V., Peixoto, F., Gomes-Laranjo, J., 2010. Bentazon triggers the promotion of oxidative damage in the Portuguese ricefield cyanobacterium *Anabaena cylindrica*: response of the antioxidant system. *Environ. Toxicol.* 25, 517–526.
- Ganzenko, O., Oturan, N., Sirés, I., Huguenot, D., van Hullebusch, E.D., Esposito, G., Oturan, M.A., 2018. Fast and complete removal of the 5-fluorouracil drug from water by electro-Fenton oxidation. *Environ. Chem. Lett.* 16, 281–286.
- Gholami, M., Shirzad-Siboni, M., Farzadkia, M., Yang, J.K., 2016. Synthesis, characterization, and application of ZnO/TiO₂ nanocomposite for photocatalysis of a herbicide (Bentazon). *Desalin. Water Treat.* 57, 13632–13644.
- Gkika, E., Kormali, P., Antonarakis, S., Dimoticali, D., Papaconstantinou, E., Hiskia, A., 2004. Polyoxometallates as effective photocatalysts in water purification from pesticides. *Int. J. Photoenergy* 6, 227–231.
- Guelfi, D.R.V., Gozzi, F., Machulek Jr., A., Sirés, I., Brillas, E., de Oliveira, S.C., 2017. Degradation of the insecticide propoxur by electrochemical advanced oxidation processes using a boron-doped diamond/air-diffusion cell. *Environ. Sci. Pollut. Res.* 24, 6083–6095.
- Guelfi, D.R.V., Gozzi, F., Machulek Jr., A., Sirés, I., Brillas, E., de Oliveira, S.C., 2018. Degradation of herbicide S-metolachlor by electrochemical AOPs using a boron-doped diamond anode. *Catal. Today* 313, 182–188.
- Islam, F., Wang, J., Farooq, M.A., Khan, M.S., Xu, L., Zhu, J., Zhou, W., 2017. Potential impact of the herbicide 2,4-dichlorophenoxyacetic acid on human and ecosystems. *Environ. Int.* 111, 332–351.
- Kearney, P.C., Muldoon, M.T., Somich, C.J., 1987. UV-ozonation of eleven major pesticides as a waste disposal pretreatment. *Chemosphere* 16, 2321–2330.
- Köck-Schulmeyer, M., Ginebreda, A., Postigo, C., Garrido, T., Fraile, J., de Alda, M.L., Barceló, D., 2014. Four-year advanced monitoring program of polar pesticides in groundwater of Catalonia (NE-Spain). *Sci. Total Environ.* 470, 1087–1098.
- Lambert, S.D., Graham, N.J.D., Croll, B.T., 1996. Degradation of selected herbicides in a lowland surface water by ozone and ozone-hydrogen peroxide. *Ozone Sci. Eng.* 18, 251–269.
- Lanzalaco, S., Sirés, I., Sabatino, M.A., Dispenza, C., Scialdone, O., Galia, A., 2017. Synthesis of polymer nanogels by electro-Fenton process: investigation of the effect of main operation parameters. *Electrochim. Acta* 246, 812–822.
- Liu, X., Zhou, Y., Zhang, J., Luo, L., Yang, Y., Huang, H., Peng, H., Tang, L., Mu, Y., 2018. Insight into electro-Fenton and photo-Fenton for the degradation of antibiotics: mechanism study and research gaps. *Chem. Eng. J.* 347, 379–397.
- Loos, R., Carvalho, R., António, D.C., Comero, S., Locoro, G., Tavazzi, S., Jarosova, B., 2013. EU-wide monitoring survey on emerging polar organic contaminants in wastewater treatment plant effluents. *Water Res.* 47, 6475–6487.
- Martínez-Huitle, C.A., Rodrigo, M.A., Sirés, I., Scialdone, O., 2015. Single and coupled electrochemical processes and reactors for the abatement of organic water pollutants: a critical review. *Chem. Rev.* 115, 13362–13407.
- Mir, N.A., Haque, M.M., Khan, A., Muneer, M., Vijayalakshmi, S., 2014. Photocatalytic degradation of herbicide Bentazon in aqueous suspension of TiO₂: mineralization, identification of intermediates and reaction pathways. *Environ. Technol.* 35, 407–415.
- Moreira, F.C., Boaventura, R.A.R., Brillas, E., Vilar, V.J.P., 2017. Electrochemical advanced oxidation processes: a review on their application to synthetic and real wastewaters. *Appl. Catal. B: Environ.* 202, 217–261.
- Murillo-Sierra, J.C., Sirés, I., Brillas, E., Ruiz-Ruiz, E.J., Hernández-Ramírez, A., 2018. Advanced oxidation of real sulfamethoxazole + trimethoprim formulations using different anodes and electrolytes. *Chemosphere* 192, 225–233.
- Oliveira, J.M., Galhano, V., Henriques, I., Soares, A.M., Loureiro, S., 2017. Basagran® induces developmental malformations and changes the bacterial community of zebrafish embryos. *Environ. Pollut.* 221, 52–63.
- Olvera-Vargas, H., Oturan, N., Oturan, M.A., Brillas, E., 2015. Electro-Fenton and solar photoelectro-Fenton treatments of the pharmaceutical ranitidine in pre-pilot flow plant scale. *Separ. Purif. Technol.* 146, 127–135.
- Oturan, N., Abdesslem, A.K., Bellakhal, N., Dachraoui, M., Oturan, M.A., 2010a. Treatment of a mixture of three pesticides by photo- and electro-Fenton processes. *Desalination* 250, 450–455.
- Oturan, M.A., Oturan, N., Abdesslem, A.K., Bellakhal, N., Dachraoui, M., 2010b. Treatment of an aqueous pesticides mixture solution by direct and indirect electrochemical advanced oxidation processes. *Int. J. Environ. Anal. Chem.* 90, 468–477.
- Panizza, M., Cersola, G., 2009. Direct and mediated anodic oxidation of organic pollutants. *Chem. Rev.* 109, 6541–6569.
- Pelizzetti, E., Maurino, V., Minero, C., Zerbini, O., Borgarello, E., 1989. Photocatalytic degradation of bentazon by TiO₂ particles. *Chemosphere* 18, 1437–1445.
- Pourata, R., Khataee, A.R., Aber, S., Daneshvar, N., 2009. Removal of the herbicide bentazon from contaminated water in the presence of synthesized nanocrystalline TiO₂ under irradiation of UV-C light. *Desalination* 249, 301–307.
- Ridrujo, C., Alcaide, F., Álvarez, G., Brillas, E., Sirés, I., 2018. On-site H₂O₂ electro-generation at a CoS₂-based air-diffusion cathode for the electrochemical degradation of organic pollutants. *J. Electroanal. Chem.* 808, 364–371.
- Rodrigues, E.T., Alpendurada, M.F., Ramos, F., Pardal, M.A., 2018. Environmental and human health risk indicators for agricultural pesticides in estuaries. *Ecotoxicol. Environ. Saf.* 150, 224–231.
- Schneider, M.V., Rosa, M.F., Lobo, V.D.S., Baricatti, R.A., 2014. Photocatalytic degradation of bentazon with TiO₂. *Eng. Sanitária Ambient.* 19, 61–66.
- Seck, E.L., Doña-Rodríguez, J.M., Fernández-Rodríguez, C., Portillo-Carrizo, Hernández-Rodríguez, M.J., González-Díaz, O.M., Pérez-Peña, J., 2013. Solar photocatalytic removal of herbicides from real water by using sol-gel synthesized nanocrystalline TiO₂: operational parameters optimization and toxicity studies. *Sol. Energy* 87, 150–157.
- Steter, J.R., Brillas, E., Sirés, I., 2016. On the selection of the anode material for the electrochemical removal of methylparaben from different aqueous media. *Electrochim. Acta* 222, 1464–1474.
- Steter, J.R., Brillas, E., Sirés, I., 2018. Solar photoelectro-Fenton treatment of a mixture of parabens spiked into secondary treated wastewater effluent at low input current. *Appl. Catal. B: Environ.* 224, 410–418.
- Thiam, A., Brillas, E., Centellas, F., Cabot, P.L., Sirés, I., 2015. Electrochemical reactivity of Ponceau 4R (food additive E124) in different electrolytes and batch cells. *Electrochim. Acta* 173, 523–533.
- Thiam, A., Salazar, R., Brillas, E., Sirés, I., 2018. Electrochemical advanced oxidation of carbofuran in aqueous sulfate and/or chloride media using a flow cell with a RuO₂-based anode and an air-diffusion cathode at pre-pilot scale. *Chem. Eng. J.* 335, 133–144.
- Thuy, P.T., Moons, K., Van Dijk, J.C., Viet Anh, N., Van der Bruggen, B., 2008. To what extent are pesticides removed from surface water during coagulation-flocculation? *Water Environ. J.* 22, 217–223.
- USEPA, NSCEP, 1998. Toxicological Review of Bentazon. Available in: <https://nepis.epa.gov/Exe/ZyPDF.cgi/P1006D3V.PDF?Dockey=P1006D3V.pdf> (last accessed 2018).
- Wei, X., Gao, N., Li, C., Deng, Y., Zhou, S., Li, L., 2016. Zero-valent iron (ZVI) activation of persulfate (PS) for oxidation of bentazon in water. *Chem. Eng. J.* 285, 660–670.
- WHO, 2017. Guidelines for Drinking-water Quality, vol. 1 Available in: http://www.who.int/water_sanitation_health/water-quality/guidelines/chemicals/bentazone-background-jan17.pdf?ua=1 (last accessed 2018).
- WWAP, 2017. The United Nations World Water Development Report 2017. Wastewater: the Untapped Resource. UNESCO, Paris.
- Zhang, Y., Wang, A., Tian, X., Wen, Z., Lv, H., Li, D., Li, J., 2016. Efficient mineralization of the antibiotic trimethoprim by solar assisted photoelectro-Fenton process driven by a photovoltaic cell. *J. Hazard. Mater.* 318, 319–328.
- Zöllig, H., Remmele, A., Fritzsche, C., Morgenroth, E., Udert, K.M., 2015. Formation of chlorination byproducts and their emission pathways in chlorine mediated electro-oxidation of urine on active and nonactive type anodes. *Environ. Sci. Technol.* 49, 11062–11069.